Statistical Analysis of Relationship between daytime Lidar-Derived Planetary Boundary Layer Height and Relevant Atmospheric Variables in the Semi-Arid Region in Northwest China

Ruijun Dang[1], Hong Li[1], Zhiguo Liu[2], and Yi Yang[1*]

[1] *Key Laboratory of Arid Climatic Changing and Reducing Disaster of Gansu Province, College of Atmospheric Sciences, Lanzhou University, Lanzhou, Gansu 730000, China*
[2] *The Central Meteorological Observatory of Lanzhou, Lanzhou, 730020, China*

Nov 9th, 2015

Submitted to *Advances in Meteorology*

Corresponding author's address:
*Yi Yang (Email: yangyi@lzu.edu.cn, Cell phone: +86-13893256933)
College of Atmospheric Sciences, Lanzhou University, No.222 TianShui South Road, Lanzhou City, Gansu Province 730000, China

Abstract

Accurate identification of key parameters for data assimilation is important to simulate the planetary boundary layer height (PBLH) and structure evolution in numerical weather prediction models. In this study, surface observational data and lidar-derived PBLH on 42 cloudless days from June 2007 to May 2008 are used to quantify the statistical relationships between surface parameters and the PBLH at a semi-arid climate observational site in Northwest China. The results indicate that surface upward long wave radiation, surface temperature, and surface sensible heat fluxes show strong correlations with the PBLH with correlation coefficients at a range of 0.63-0.72. But these parameters show varying correlation response time to the different stages of PBL development. Furthermore, the air temperature shows the highest correlation with the PBLH near the surface and the correlation decreases with increasing height.

1. Introduction

The atmospheric boundary layer, also known as the planetary boundary layer (PBL) is the turbulent layer near the Earth's surface. It is directly affected by the underlying surface conditions and intimately associated with human activity [1]. In this layer, the atmosphere is always in a turbulent status. The turbulence causes the transfers of momentum, heat, and moisture between the surface and atmosphere. So the PBL is crucial to surface–atmosphere exchanges of substances and energy. PBLH is of major relevance in boundary layer research as a key parameter characterizing the structure of the boundary layer [2, 3]. Observations of the PBLH are significant for theory and applications. It is closely related to turbulence. Accordingly it is not observed by standard measurements and there is no such device as the PBL meter. It is currently determined mainly from indirect measurements. Under clear conditions when atmosphere is in neutral or unstable, wind velocity and potential temperature are well mixed in the PBL. In most cases, they are usually constants in this layer. So the PBL is also known as the mixing layer. However, there is a sharp increase in wind speed and potential temperature caused by the abrupt decrease in turbulence intensity at the top of mixing layer [4]. The characteristics of wind speed and potential temperature can be used to calculate the PBLH. Also, the PBL is moist relative to the upper free atmosphere, and a strong gradient in relative humidity exists at the top of PBL, which can also be used to determine the PBLH [5]. So the PBLH can be determined from different instruments-derived profiles of thermodynamic variables like temperature, humidity, and horizontal wind speed, however, only infrequently. The difficulty in directly observing the thermodynamic structures of the atmosphere makes ground-based remote sensing technique an attractive choice. For instance, lidar provides vertical profiles of backscatter from aerosol particles with high temporal and spatial resolution in the atmosphere. The aerosol concentration within the PBL is much higher than that in the free atmosphere. Therefore, a significant difference in aerosol concentration exists between the top of the PBL and the free atmosphere, which is reflected in the lidar echo signals as a sudden attenuation of the signal. On the basis of this characteristic of aerosols in the PBL, aerosol particles can be used as tracers to determine the PBLH. However, in the presence of optically thick clouds, the resulting PBLH using lidar data is unrealistic because of the high signal gradient generated by the clouds [6, 7]. Therefore, in this paper clear sky conditions are chosen to calculate PBLH from lidar data.

Retrieving PBLH from lidar data uses the gradient of the aerosol particle concentration, as the backscatter signal generally decreases most rapidly at the top of the boundary layer. Many methods have been used to obtain the PBLH from backscatter intensity, including the gradient method [8-10], the wavelet transform method [11-13], the standard deviation method [14], and the curve fitting method [15, 16]. Each method has its advantages and limitations. The gradient method is simple and easy to use, but rather sensitive to local minima in the profile either atmosphere- or noise-induced which nearly always occur in a turbulent PBL [17]. The standard deviation method is not suitable for the situation of weak inversion layer [18]. Although the curve fitting method is relatively computationally expensive, it is barely affected by the local structure of the signal, and generally get stable results. Therefore, curve fitting method is the best one for batch processing of large amounts of data [16], and it is used to retrieve daytime PBLH in this paper.

The atmospheric boundary layer is largely governed by land surface processes, including the absorption of solar radiation by the land surface, transmission of heat energy to the atmosphere and soil, and mechanical processes. The surface temperature is an important external forcing factor on the thermal convection. Besides, the variation in surface temperature reflects the heating result of net radiation on the surface [19]. For net radiation, contribution of the long- and short-wave components varies with atmospheric conditions. On sunny days, the upward long wave contributes most to the net radiation, and contribution of upward shortwave is minimum [20]. Besides, the development and maintaining of the thermal boundary layer mainly rely on the heat transmission through the sensible heat flux [21]. Therefore, the radiation variables, surface temperature and sensible heat flux make major contributions to the formation and development of the PBL [22-25]. It may update the initial fields of these variables with PBLH assimilation into numerical model.

For PBLH assimilation in the numerical model with Ensemble Kalman Filter (EnKF), it need to confirm which variables are well correlate with PBLH. In addition, the influence radius for spatial and temporal are also should be set. So the focus of study is to find out the statistical correlation between PBLH and conventional atmospheric variables using the routine observations at the Semi-Arid Climate and Environment Observatory of Lanzhou University (SACOL), then provide basis and support for PBLH assimilation in northwest China. By the limits of the single observational point, we couldn’t find out the radius of influence in horizontal direction. For the vertical direction, we did the work using the vertical air temperature profile provided by a Radiometrics profiling radiometer (TP/WVP-3000). The observations of variables and PBLH later some hours are used to analyze the influence radius in time.

Considering the above, the works are as follows: 42 cloudless sunny days (non-precipitation, without thunderstorm, no cloud or total-cloud covers is less than 20 percent all day and with a clear structure of backscatter signals of lidar) are selected from June 2007 to May 2008, and the PBLH is calculated by retrieving lidar data using the curve fitting method over the Lanzhou suburb in the Yuzhong area at SACOL. The correlations between averages of variables and PBLH, as well as lagged correlations between time series of variables and PBLH are calculated, to determine the major variables affecting the formation and development of boundary layer, the correlation coefficients of PBLH and air temperature at different heights are also calculated. Finally, taking 15 July 2007, 20 November 2007, 5 January 2008 and 9 April 2008 as typical examples in different seasons, we investigate the temporal variations in PBLH and variables, and discuss specifically how the atmospheric variables affect the development of the boundary layer and the time it takes for the boundary layer to react to changes in the driving variables in different seasons.

2. Data and methods

The PBLH and statistical correlations in this paper are calculated from data collected at SACOL (35.946°N, 104.137°E; 1961 m above sea level), which is near the city of Lanzhou on the southern bank of the Yellow River, in a typical semi-arid region. The instruments include air temperature and relative humidity (HMP45CL,Vaisalla), a Precision Infrared temperature radiometer (IRTS-P, Apogee), upward and downward pyranometers (CM21, Kipp & Zonen), upward and downward pyrgeometers (CG4, Kipp & Zonen), an atmospheric Pressure Sensor (RPT410F-3143, Druck), a Radiometrics Profiling Radiometer (TP/WVP-3000, Radiometrics), and a Micro-Pulse Lidar system (MPL-4, Sigma Space). The vertical spatial resolution of the radiometer providing air temperature profiles is 100 m below 1 km and 250 m above 1 km. The MPL-4 has one measurement channel at 527 nm, which records backscatter signals up to a height of 30 km with a vertical resolution of 75 m. All the conventional atmospheric observations are subjected to basic quality control (QC). Only observations with a relatively high accuracy are selected. The SACOL MPL-4 has joined the MPLNET (Micro-Pulse Lidar Network) [26], and the observation follows the relevant uniform rules. Meanwhile, a series of corrections such as background correction, overlap correction and range correction have been done to lidar data [27].

The curve fitting method first proposed by Steyn [17] is used to retrieve PBLH from the lidar data. The technique uses the gradient of the lidar backscatter signal and fits an idealized backscatter profile $B(z)$ to the observed backscatter profile $b(z)$ by minimizing the measure of agreement between the two profiles. The form of the idealized backscatter profile $B(z)$ is

$$\mathrm{B(z)} = \frac{(\mathrm{B_m + B_u})}{2} - \frac{(\mathrm{B_m - B_u})}{2}\mathrm{erf}\left(\frac{\mathrm{z - Z_m}}{\mathrm{S}}\right) \quad (1)$$

The error function (erf) defined as:

$$\mathrm{erf(a)} = \frac{2}{\sqrt{\pi}}\int_0^a \exp(-\mathrm{z}^2)\mathrm{dz} \quad (2)$$

Where B_m and B_u are the mean backscatter in the mixed layer and in air immediately above the mixed layer, respectively; Z_m is the depth of the mixed layer; S is related to the thickness of the entrainment layer [28]. The four parameters are determined by minimizing the root-mean-square deviation between $B(z)$ and $b(z)$. When the root-mean-square deviation gets the minimum, Z_m represents PBLH.

3. Statistical correlations between PBLH and variables

3.1. Statistical correlations between averages. The dates chosen for PBLH retrieval and correlation analysis are listed in Table 1. On these 42 cloudless sunny days, conventional observations are complete; the lidar backscatter signals also have clear structure. To ensure representativeness, the selected days are from all four seasons. Because some data are unavailable for 8–30 September 2007, the cases in autumn are relatively less. But the representativeness of the statistical correlations aren't be affected.

TABLE 1: Selected days for retrieving PBLH and for correlation analysis between PBLH and atmospheric variables from June 2007 to May 2008

June.	July	Aug.	Nov.	Dec.	Jan.	Feb.	Mar.	Apr.	May.
1	15	14	20	19	5	20	1	2	4
9	16	16	22	20	9	21	3	4	5
	22	19	28	22	15		13	6	11
		31	30				25	9	14
							26	17	26
								24	28
								25	31
								27	
								28	

Table 2 lists the Pearson correlation coefficients of the averages of different variables and PBLH during 10:00 and 18:00 (Local standard time). It shows strong correlations between individual thermal variables (e.g., surface air temperature, surface temperature, sensible heat flux and upward and downward long wave and shortwave radiation) and PBLH, with correlation coefficients all around 0.6 (significant at the 0.01 level). Surface relative humidity and atmospheric pressure are negatively correlated with PBLH but their relevance is relatively low (r = –0.339 and –0.247, respectively). The weakest correlation is between net radiation and PBLH. Figure 1 shows the distribution of averages of variables and PBLH. It can be seen that the daily average of net radiation changes very little, while the PBLH shows a clear change (see Figure 1 b). The overall trends of atmospheric pressure and surface relative humidity are generally opposite to that of PBLH although they change in tandem with PBLH sometimes (see Figure 1 c). Apart from these three variables, Figure 1 shows that the overall trends are fairly consistent with the trend of PBLH.

TABLE 2: Statistical correlations between the averages of atmospheric variables and boundary layer height from 10:00 to 18:00 (T0: surface air temperature; Ts: surface temperature; H: sensible heat flux; RH: surface relative humidity; P: atmospheric pressure; R_{lu}, R_{su}, R_{ld}, R_{sd}: upward long wave and shortwave radiation, and downward long wave and shortwave radiation, respectively; R_n: net radiation; *r*: Pearson correlation coefficient)

variables	*r*
T0	0.707**
Ts	0.711**
H	0.629**
RH	-0.339*
P	-0.247
R_{lu}	0.753**
R_{ld}	0.545**
R_{sd}	0.764**
R_{su}	0.599**
R_n	-0.043

*Significant correlation at the 0.05 significance level

**Significant correlation at the 0.01 significance level

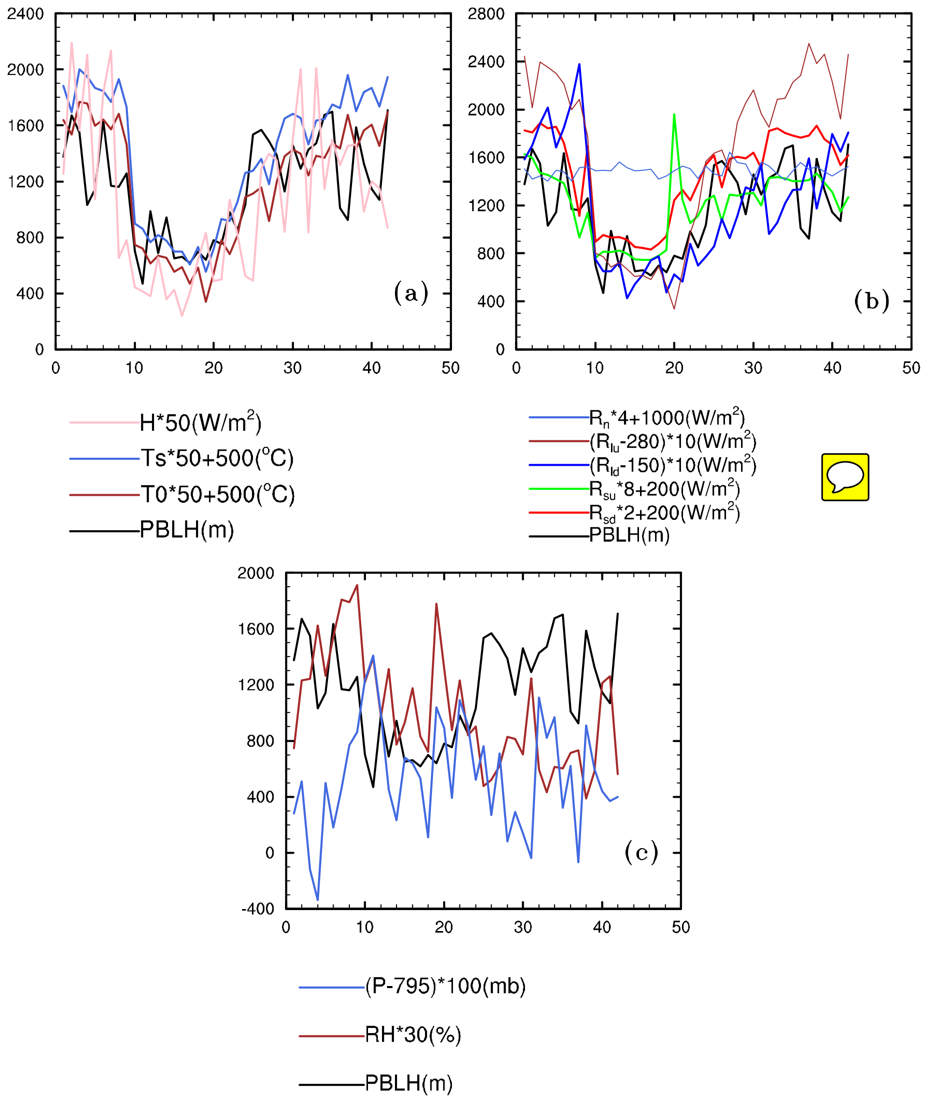

FIGURE 1: Distribution of averages of atmospheric variables and boundary layer height (see Table 2 for abbreviations).

3.2. Statistical correlations between time series. In general, the atmospheric boundary layer appears as a daytime convective layer and a stable boundary layer at night. As discussed by Ding [29] that the boundary layer with a thick mixed layer is relatively stable before sunrise in northwest China. After 08:00, the nighttime stable boundary layer is broken; the mixed layer starts to deepen. Around 10:00, because of thermally driven vertical mixing, the residual layer starts to disappear and the mixed layer begins to develop rapidly. By noon, the convective boundary layer is established. Zhao [30] estimated the PBLH in summer over the SACOL using lidar measurements and a numerical model, and showed that the deepest boundary layer over SACOL occurs at around 17:00 and can last until 18:00. Therefore, PBLH is selected every 30 minutes during 10:00–18:00, and atmospheric variables are selected during 06:00–14:00, 07:00–15:00, 08:00–16:00, 09:00–17:00, and 10:00–18:00 as time series to analyze the lagged statistical correlations between variables and PBLH, as the boundary layer often develops after changes in these variables.

Statistical correlations between different atmospheric variables and PBLH with a lag of 1, 2, 3, and 4 hours are listed in Table 3. There are significant correlations between thermal variables (except net radiation) and PBLH, with Pearson correlation coefficients all above 0.6 (significant at the 0.01 level), which is highly consistent with the results shown in Table 2. It is also clear that stronger significant correlations exist between variables and the PBLH 2–3 hours later. The Pearson correlation coefficients between surface temperature, surface air temperature and PBLH 2 hours later are 0.704 and 0.677, respectively. Upward long wave radiation, upward shortwave radiation, and downward shortwave radiation are more highly correlated with PBLH 3 hours later. The correlation coefficients are 0.723, 0.687, and 0.608, respectively. Downward long wave radiation is different from the others. It is more highly correlated with PBLH at the same time. Besides, with the correlation coefficient of 0.629, sensible heat flux highly correlates with PBLH at the same time or later about 1 hour. The weakest correlation of the radiation variables is between net radiation and PBLH, the strongest correlation is with PBLH 3 hours later. Atmospheric pressure and surface relative humidity are both negatively correlated with PBLH, although the correlation is not as significant as the case of the thermal variables. For lagging effect, the PBLH changes about 2 hours after a change in relative humidity.

TABLE 3: Statistical correlations between different atmospheric variables and boundary layer height at lag time of 1–4 hours (T0: surface air temperature; Ts: surface temperature; H: sensible heat flux; RH: surface relative humidity; P: atmospheric pressure; R_{lu}, R_{su}, R_{ld}, R_{sd}: upward long wave and shortwave radiation, and downward long wave and shortwave radiation, respectively; R_n: net radiation; *r*: Pearson correlation coefficients)

Variables	At same time r	PBLH later 1 h r	PBLH later 2 h r	PBLH later 3 h r	PBLH later 4 h r
T0	0.647**	0.667**	0.677**	0.677**	0.666**
Ts	0.677**	0.697**	0.704**	0.701**	0.684**
H	0.629**	0.627**	0.605**	0.570**	0.518**
RH	-0.414**	-0.428**	-0.427**	-0.412**	-0.374**
P	-0.311**	-0.290**	-0.251**	-0.202**	-0.156**

R_{lu}	0.569**	0.669**	0.716**	0.723**	0.709**
R_{ld}	0.507**	0.506**	0.499**	0.480**	0.461**
R_{sd}	0.285**	0.544**	0.676**	0.687**	0.657**
R_{su}	0.170**	0.406**	0.565**	0.608**	0.602**
R_n	-0.147**	0.179**	0.403**	0.452**	0.428**

*Significant correlation at the 0.05 significance level

**Significant correlation at the 0.01 significance level

To identify any relations and influence radius in the vertical direction, Table 4 shows the statistical correlations between PBLH and air temperature at different heights for different times. At 10:00, only air temperature below 1000 m is correlated with PBLH, but after 12:00, air temperature within 5000 m is significantly correlated with PBLH. Thermal forcing is the driving force for the development of mixing layer in daytime (10:00-18:00). However, only small amount of solar radiation is absorbed by air in the boundary layer, most (about 90%) are delivered to the surface. In turn it forces PBL development through turbulent transport. In vertical direction, the forcing effect of surface decreases with height, and temporal variation in air temperature at higher altitude is less significant [1]. So the Pearson correlation coefficient is highest at the surface and decreases with height at all times (see Table 4). Furthermore, the highest correlation between PBLH and air temperature below (above) 1000 m occurs at 12:00 (14:00), the Pearson correlation coefficient is 0.748 (0.637). In addition, for the whole troposphere, the ground surface is the main heat source, the air temperature in the free atmosphere changes with the surface variation. So at 14:00, there is relative higher correlation between PBLH and air temperature at 5 km or more.

TABLE 4: Statistical correlations between PBLH and air temperature at different heights and at different times (r: Pearson correlation coefficient)

Height (m)	10:00 r	12:00 r	14:00 r	16:00 r	18:00 r
0	0.565**	0.748**	0.655**	0.638**	0.627**
100	0.545**	0.739**	0.655**	0.639**	0.617**
200	0.532**	0.727**	0.654**	0.632**	0.608**
300	0.519**	0.718**	0.653**	0.623**	0.601**
400	0.481**	0.708**	0.652**	0.610**	0.590**
500	0.446**	0.697**	0.647**	0.599**	0.582**
600	0.412**	0.683**	0.644**	0.585**	0.571**
700	0.385*	0.668**	0.642**	0.573**	0.558**
800	0.360*	0.654**	0.640**	0.563**	0.548**
900	0.341*	0.641**	0.639**	0.553**	0.539**
1000	0.322*	0.629**	0.637**	0.540**	0.529**

1250	0.275	0.592**	0.628**	0.5000**	0.496**
1500	0.252	0.575**	0.625**	0.477**	0.478**
1750	0.256	0.573**	0.627**	0.478**	0.475**
2000	0.255	0.565**	0.625**	0.470**	0.469**
2250	0.254	0.558**	0.624**	0.462**	0.460**
2500	0.257	0.557**	0.623**	0.458**	0.456**
2750	0.249	0.547**	0.618**	0.447**	0.446**
3000	0.256	0.551**	0.620**	0.447**	0.448**
3250	0.245	0.539**	0.611**	0.431**	0.432**
3500	0.247	0.537**	0.609**	0.427**	0.427**
3750	0.242	0.531**	0.604**	0.417**	0.419**
4000	0.251	0.534**	0.604**	0.420**	0.422**
4250	0.252	0.533**	0.600**	0.416**	0.419**
4500	0.250	0.530**	0.598**	0.412**	0.414**
4750	0.246	0.527**	0.595**	0.407**	0.409**
5000	0.247	0.528**	0.594**	0.408**	0.409**

*Significant correlation at the 0.05 significance level

**Significant correlation at the 0.01 significance level

4. Cases analysis

To verify the statistical results and analyze the roles played by atmospheric variables in the development of the boundary layer, four cloudless sunny days from different seasons, 09 April 2008, 15 July 2007, 20 November 2007 and 5 January 2008 , are selected as typical spring, summer, fall and winter examples for analysis.

4.1 Synoptic condition. Besides surface processes, synoptic condition is also an important factor contributing to the overall height of boundary layer. The surface pressures at 14:00 for four cases are shown in figure 2. And figure 3 shows the time–altitude cross-section of the backscatter intensity, the red line represents retrieved PBLH with the curve fitting method. After 10:00, PBLH begin to increase on all cases, higher PBLH appear before 10:00 on 9 April 2008 and 15 July 2007 (Figure3 (a), (b)), which may be caused by cloud or the limitation of the method. It can be seen from Figures 2 (a) and (b) that, Yuzhong region is controlled by weak low-surface pressure at 14:00 on 9 April 2008 and 15 July 2007. In these cases, the updrafts promote PBL development. According to Figure 3 (a) and (b), the highest PBLH are 1850 m and 2150 m on the two cloudless sunny days, respectively. They are relative higher than on other two cases. It also can be seen that the area is controlled by the edge of high-pressure system at 14:00 on 20 November 2007 and 5 January 2008 from Figures 2 (c) and (d), which indicating aloft airflow convergence and surface divergence. In those cases, the PBL developments are subsided and restricted, the highest PBLH are 1100m and 860 m, respectively (see Figures 3 (c) and (d)). Meanwhile, Figure 3 also shows the time that PBLH get the maximum. The times that peak values appear are 17:30, 15:30, 17:00 and 17:00, respectively. It is not difficult to understand that the difference on temporal variation in PBLH is closely related to the differences on the land surface processes and the variation in atmospheric variables. In addition, the difference between the height at which the signal reduced fastest and the PBLH (retrieved with the curve fitting method) is small (Figure 3), the corresponding time is also fairly consistent, which supports the choice of the curve fitting method for retrieving PBLH on sunny days.

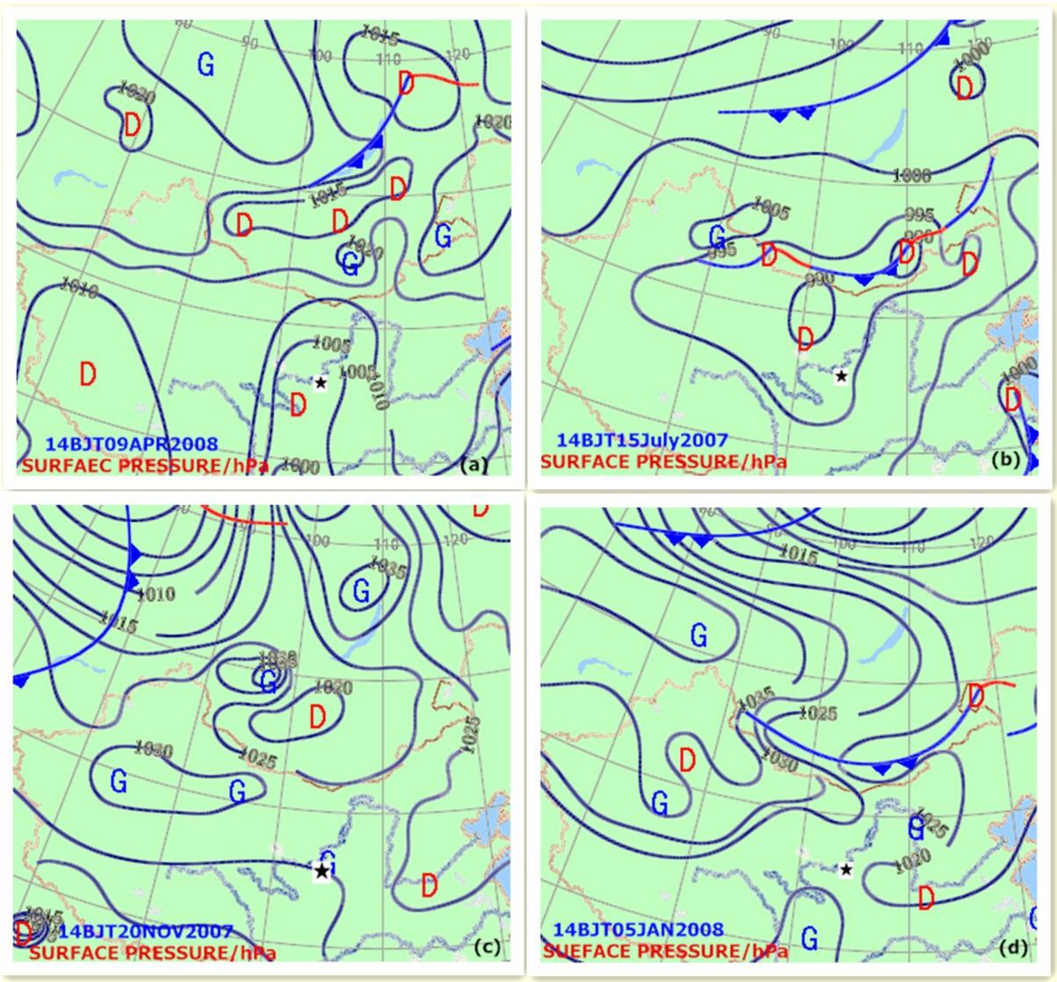

FIGURE 2: Surface pressure at (a) 14:00 BJT 9 April 2008, (b) 14:00 BJT 15 July 2007, (c) 14:00 BJT 20 November 2007, and (d) 14:00 BJT 5 January 2008. Black star denotes measurement site.

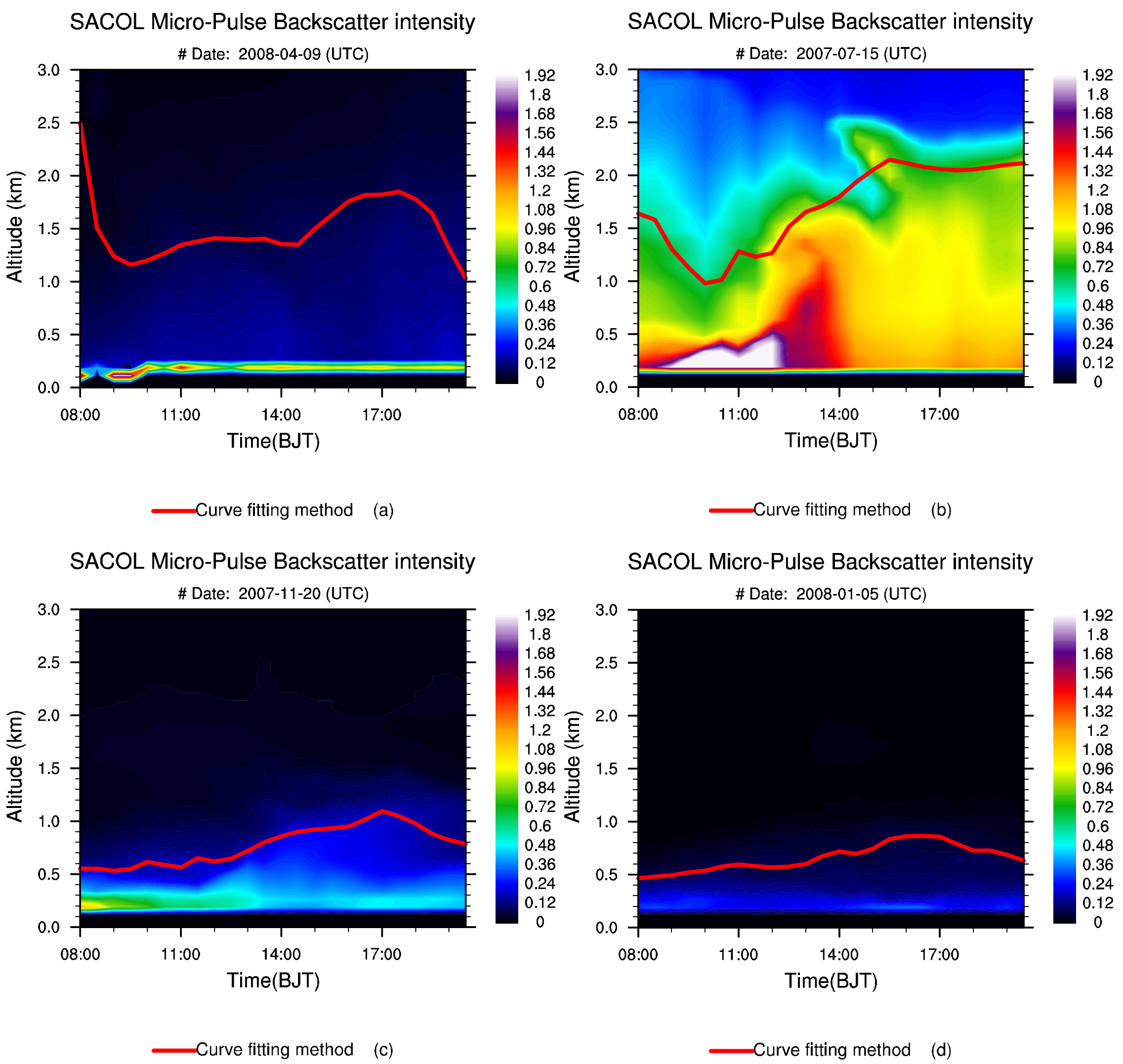

FIGURE 3: Time–altitude cross-sections of the backscatter on (a) 9 April 2008, (b) 15 July 2007, (c) 20 November 2007, and (d) 5 January 2008.

4.2 Temporal variation analysis. The temporal variations in radiation variables are plotted in Figure 4. The downward shortwave radiation is the part of the solar radiation that reaches the surface after attenuation through the atmosphere. Then some is absorbed by the surface and the rest is reflected back into the atmosphere, which is upward shortwave radiation. Therefore, to all cases, the upward shortwave radiation always accompany the downward component. From Figure 4, it is obvious that on the first two cases, short wave radiation have higher values than on the 20 November 2007 and 5 January 2008, which are caused by the seasonal variation of solar altitude angles (atmospheric transparency is not considered in cloudless sunny days). Except the synoptic condition, shortwave radiation contributes to the difference on PBLH to a certain extent as the ultimate source of energy.

Besides, for temporal variation, the downward and upward shortwave radiation reach their maximum values between 12:30 and 13:30, and then decrease rapidly. Although the temporal variations in shortwave radiation for all cases are similar, significant difference exit at the development and lag time of PBLH for different cases. The lag time of PBLH is less than 3 hours on 15 July 2007, while more than 3 hours for other three cases. Maybe differences on land process in different seasons contributes to the difference on the lag law of PBLH.

The upward long wave radiation change 0.5 to 1 hour later than the shortwave radiation, this is because upward long wave radiation depends on surface temperature, and the various processes occurring from the arrival of solar radiation at the surface to the surface reaching its maximum temperature take some time. Obviously, for the case of 15 July 2007, the value of the upward long wave radiation is biggest, and on the case of 5 January 2008 is smallest. On other two cases, the values are somewhere in between. The peak values occur between 13:30 to 14:30, indicating that the lag times of PBLH are 3.5, 1.5, 3.5 and 2.5 hours, respectively. The temporal variation in downward long wave radiation is different from other radiation components. To all cases, the variable increases until about 18:00 or after 17:00 the decreasing tendency begins to appear. Besides, the temporal variation range of downward long wave radiation is also smaller than others. The atmosphere absorbs both shortwave and long wave radiation, but mainly long wave radiation: only 15%–25% of the shortwave radiation is absorbed. After greenhouse gases such as water vapor and carbon dioxide in atmosphere absorbed the long wave radiation, the atmosphere is exothermic and downward long wave radiation generates. So the radiation variable often reach to the peak value latest. Meanwhile, the downward long wave radiation is strongly influenced by cloudiness and air humidity. On cloudless sunny days, the intensity of downward long wave radiation is relatively low and has a weak effect on surface heating. Accordingly, Table 3 shows that downward long wave radiation is weaker related to PBLH than the other three radiation variables.

Figure 4 also shows net radiation, being different from the profile of daily average in Figure 1, it has an obvious daily variation and changes consistently with shortwave radiation on all cases. The variation in net radiation is the cumulative results of the components' variation in the radiation balance, but the shortwave radiation is the dominant variable. Therefore, the lagged law between net radiation and PBLH for different cases is similar to that between the shortwave radiation and

PBLH. The major factors that affect the net radiation are solar altitude angles, altitude, cloud cover and surface albedo. The altitude and cloud cover are not considered in the study for cloudless sunny days, the variation in solar altitude angles is the fundamental factor to the difference on net radiation on different cases [31].

Figure 5 shows temporal variations in surface air temperature, surface infrared temperature, sensible heat flux and surface wind speed. Relative to two temperature variables, PBLH shows significant lag except on the case of 15 July 2007. On 17 April 2008, 20 November 2007 and 1 January 2008, the lag time is about 1, 2 and 2 hours, respectively. On 15 July 2007, two profiles increase until about 17:00 and then begin to decrease, which are in line with the trend of PBLH. In summer, turbulent exchange is stronger and heat exchange between surface and atmosphere is faster, so the lag effect of PBLH does not show very well. The temporal variation in sensible heat flux (SHF) is different from others, especially on the previous two cases it even changes simultaneously with PBLH, on 20 November 2007 and 5 January 2008, PBLH changes about 1 hour later than the variable. The sensible heat flux is mainly determined by difference between surface temperature, surface air temperature, and surface wind speed. According to Figure 5, the sensible heat flux changes a little time later than the difference between surface temperature and surface air temperature, but wind speed (red lines) keep increasing until 18:00, which leads to the less lag time between PBLH and sensible heat flux. Besides that, the sensible heat is calculated through surface air temperature, surface temperature and surface wind speed, the accumulated error is inevitable.

The temporal variations in atmospheric pressure and surface relative humidity are shown in Figure 6, opposite to the variation in PBLH. A comparison with the surface air temperature in Figure 5 shows that the air temperature reach its maximum at the same time as relative humidity reach its minimum, and the two quantities are highly negatively correlated. Similarly, the lag time is about 1, 2, 2 hours on 17 April 2008, 20 November 2007 and 1 January 2008 respectively. On 15 July 2007, both variables decrease until about 16:00 when relative humidity maintain its minimum and the tendency of the growth appear at about 17:00, while pressure keep decreasing until 18:00. In addition, because the atmospheric pressure changes weakly, the correlation between it and PBLH is not as strong as between PBLH and other variables.

The above results show that on all cases in different seasons, the temporal variations in all variables correspond well to that of PBLH, with upward long wave radiation, surface temperature, and surface air temperature having the closest correspondence. In time domain, difference exits at lag time of PBLH among different cases, which is mainly caused by the seasonal variation in solar altitude angles. In addition, turbulent exchange intensity is different in different seasons. However, on the whole, to most variables, the lag time of PBLH is about 2 to 3 hours. PBLH changes about 3 hours later than shortwave radiation and net radiation. To upward long wave radiation, PBLH lags 2.5-3 hours. Relative to surface temperature, surface air temperature and surface relative humidity, PBLH develops about 2 hours later. Besides, PBLH changes 1 hour or less lately than sensible heat flux, while atmospheric pressure changes consistently with PBLH to all cases. The delays in boundary layer response are related not only to the finite response times of the distribution, transformation, and transmission in the atmosphere for surface radiation energy, but also to the lag in aerosol delivery. Using lidar data, PBLH is identified by the vertical distribution of aerosol. However, upward transport of aerosol only begins after sunrise, when the boundary layer has developed in response to thermodynamic factors. In the afternoon, the true PBLH declines rapidly with the weakening of solar radiation, but the PBLH retrieved from the profile of aerosol decreased slowly. In addition, delays in PBLH may also reflect the influence of dynamical factors such as wind shear. Northwest China is in a region dominated by westerlies, and the atmospheric circulation background that influences the formation and development of the boundary layer has some special characteristics [32]. However, the correlation between wind shear and PBLH is not considered because of the limitations of the wind data.

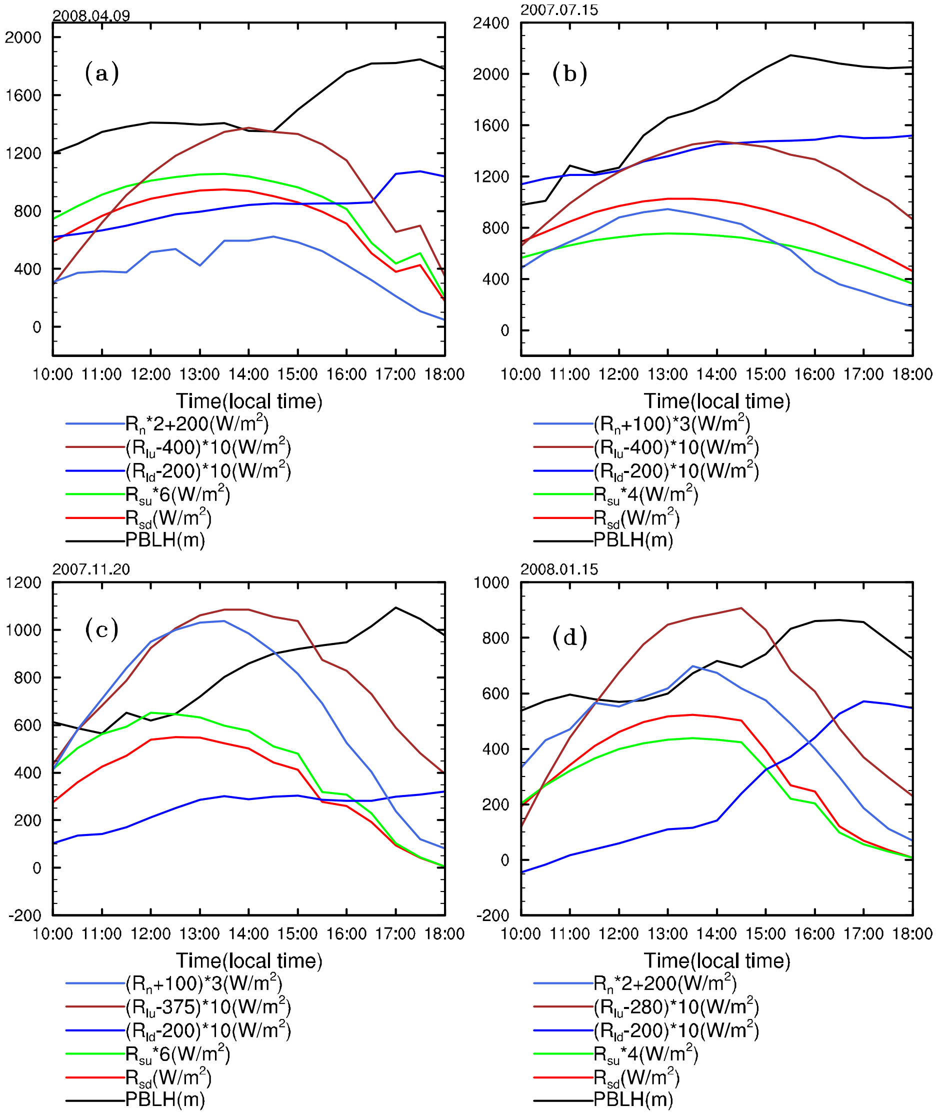

FIGURE 4: Temporal variations in boundary layer height (PBLH), downward shortwave radiation (R_{sd}), upward shortwave radiation (R_{su}), downward long wave radiation (R_{ld}), upward long wave radiation (R_{lu}), and net radiation (R_n) on (a) 9 April 2008, (b) 15 July 2007, (c) 20 November 2007, and (d) 5 January 2008.

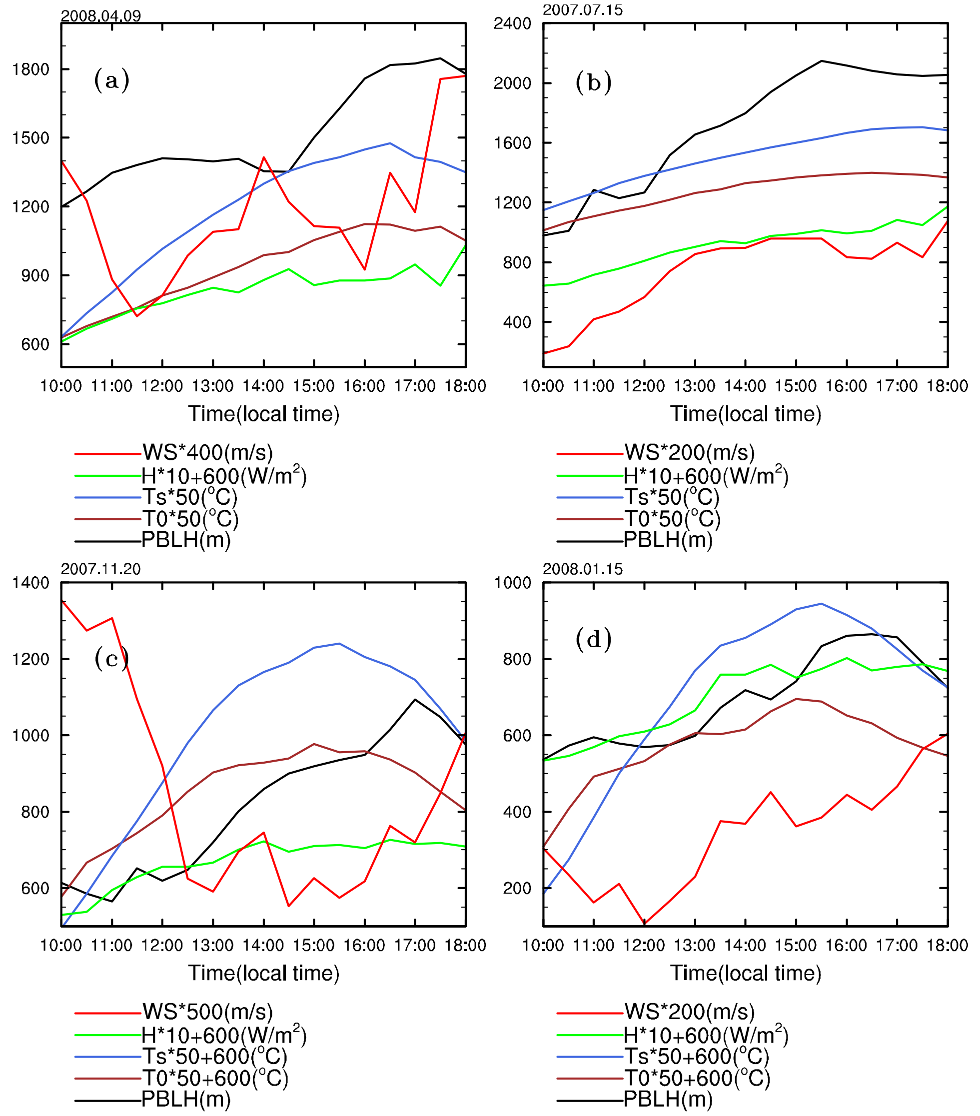

FIGURE 5: Temporal variations in boundary layer height (PBLH), sensible heat flux (H), surface temperature (Ts), surface air temperature (T0) and surface wind speed (WS) on (a) 9 April 2008, (b) 15 July 2007, (c) 20 November 2007, and (d) 5 January 2008.

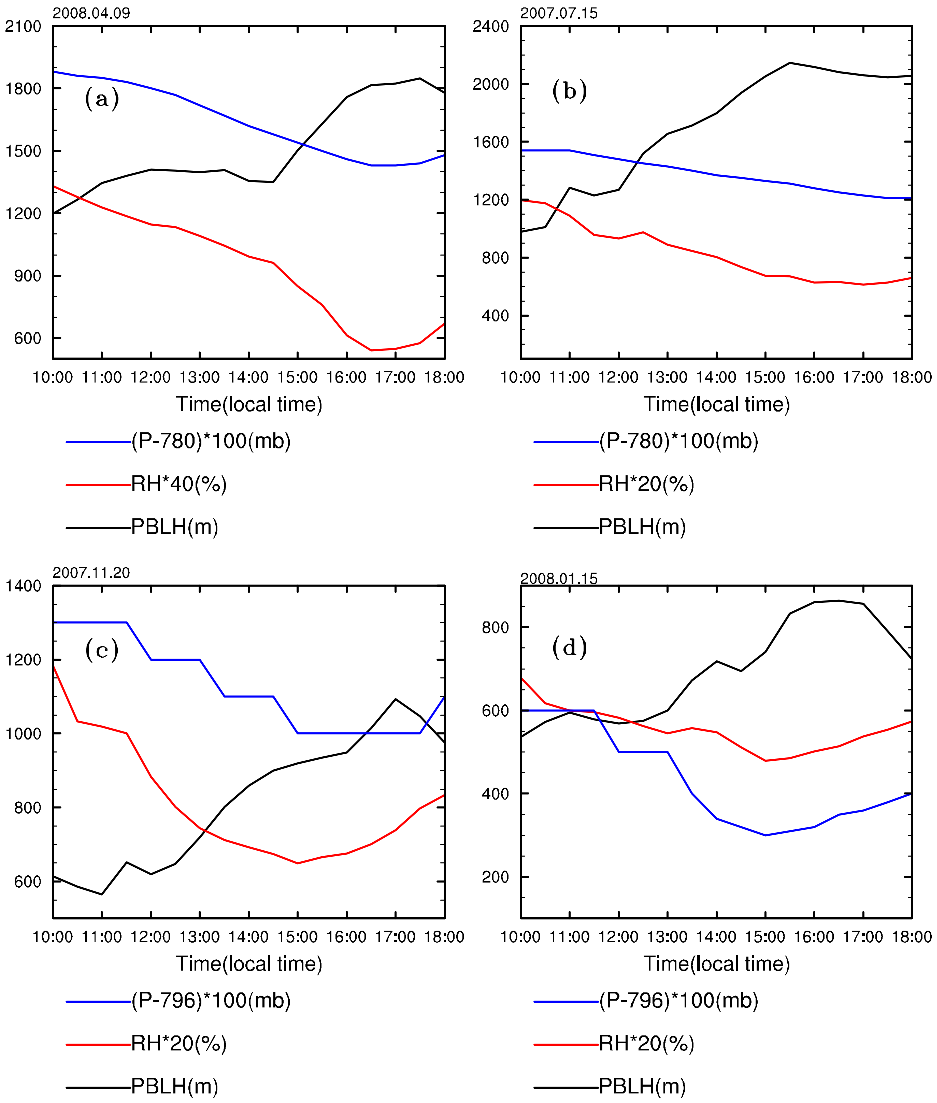

FIGURE 6: Temporal variations in boundary layer height (PBLH), surface relative humidity (RH), and atmospheric pressure (P) on (a) 9 April 2008, (b) 15 July 2007, (c) 20 November 2007, and (d) 5 January 2008.

5. Conclusions

In this study, the statistical relationships between surface parameters and the PBLH are quantified using surface observational data and lidar-derived PBLH on 42 cloudless days from June 2007 to May 2008. Meanwhile, the vertical dependence of PBLH on air temperature is also investigated. Then, using four typical cases in different seasons studies 15 July 2007, 20 November 2007, 5 January 2008 and 9 April 2008, the variables responsible for the development of the boundary layer and the lagged correlations between temporal changes of these variables and PBLH are investigated. The conclusions of the study are as follows.

(1) Among the atmospheric variables (not including dynamic factors), thermal variables such as radiation variables surface temperature and sensible heat flux have more significant positive correlations with PBLH. The response time to thermal forcing of the surface and atmosphere, together with aerosol transmission delay, means that the development of the boundary layer lags behind changes in the driving variables, with different lag times for different variables.

(2) On different cases, the lag correlation laws between PBLH and variables are different (especially on 15 July 2007), but on the whole, only downward long wave radiation changes synchronous with PBLH. Changes in the boundary layer occur 3 hours later than changes in downward, upward shortwave radiation, upward long wave radiation and net radiation. The lag time of PBLH is about 2 hours relative to surface temperature and surface air temperature, and PBLH lags about 1 hour than surface sensible heat flux.

(3) Surface relative humidity and atmospheric pressure are weaker negatively correlated with PBLH, PBLH changes about 2 hours later than surface relative humidity.

(4) The vertical dependence of PBLH on air temperature is greatest near the surface and decreases with height. The most significant correlation between air temperature below (above) 1000 m and PBLH occurs at 12:00 (14:00).

While these conclusions are important, there are still many unresolved problems. Firstly, curve fitting is an effective method for calculating PBLH from lidar data, but is limited to cloudless sunny days. The number of days and their seasonal distribution are constrained by data availability, so while the statistical results are representative they also have some limitations. Secondly, although wind shear, a major dynamical factor, affects the thermal transmission and diffusion capacity of the atmosphere and is significantly correlated with the development of the boundary layer in theory, it is not considered here because of the limited amount of data available. This analysis focus on finding out the statistical correlation between PBLH and conventional atmospheric variables according to the directly routine observations at SACOL to provide basis and support for the assimilation of PBLH in northwest China, it is not possible enough to comprehensively characterize the meteorological conditions affecting the development of the boundary layer in the Yuzhong area.

Conflict of Interests

The authors declare that there is no conflict of interests of regarding the publication of this paper.

Acknowledgements

We would like to thank the Semi-Arid Climate and Environment Observatory of Lanzhou University (SACOL) for providing the observation data. This research was supported by the National Natural science Foundation of China (Grant no. 41375109) and Arid Meteorology science Foundation of Institute of Arid Meteorology, China Meteorological Administration (Grant no. IAM201513).

References

[1] R. B. Stull, *An introduction to boundary layer meteorology*, Springer Science & Business Media, 1988.

[2] Q. Zhang, "Review of Atmospheric Boundary Layer Meteorology," *Arid Meteorology*, vol. 21, no. 3, pp. 0074-0078, 2003.

[3] X. M. Hu, J. W. Nielsen-Gammon, and F. Zhang, "Evaluation of three planetary boundary layer schemes in the WRF model," *Journal of Applied Meteorology and Climatology*, vol. 49, no. 9, pp. 1831-1844, 2010.

[4] S. E. Gryning, E. Batchvarova, "Parametrization of the depth of the entrainment zone above the daytime mixed layer," *Quarterly Journal of the Royal Meteorological Society*, vol. 120, no. 515, pp. 47-58,1994,

[5] A. B. White, C. W. Fairall and D. W. Thomson, "Radar observations of humidity variability in and above the marine atmospheric boundary layer," *Journal of Atmospheric and Oceanic Technology*, vol. 8, no. 5, pp. 639-658, 1991.

[6] K. J. Davis, N. Gamage, C. R. Hagelberg et al., "An objective method for deriving atmospheric structure from airborne lidar observations," *Journal of Atmospheric and Oceanic Technology*, vol. 17, no. 11, pp,1455-1468,2000.

[7] B. Hennemuth and A. Lammert, "Determination of the atmospheric boundary layer height from radiosonde and lidar backscatter," *Boundary-Layer Meteorology*, vol. 120, no. 1, pp. 181-200, 2006.

[8] K. L. Hayden, K. G. Anlauf, R. M. Hoff et al., "The vertical chemical and meteorological structure of the boundary layer in the Lower Fraser Valley during Pacific'93," *Atmospheric Environment*, vol. 31, no. 14, pp. 2089-2105, 1997.

[9] V. Wulfmeyer, "Investigation of turbulent processes in the lower troposphere with water vapor DIAL and radar-RASS," *Journal of the atmospheric sciences*, vol. 56, no. 8, pp. 1055-1076, 1999.

[10] J. Huang and J. Wu, “MW-FRA and its pump optimization,” *Study of Optical Communication*, no. 2, pp. 53-55, 2005.

[11] S. A. Cohn and W. M. Angevine, “Boundary layer height and entrainment zone thickness measured by lidars and wind-profiling radars,” *Journal of Applied Meteorology*, vol. 39, no. 8, pp. 1233-1247, 2000.

[12] I. M. Brooks, “Finding boundary layer top: Application of a wavelet covariance transform to lidar backscatter profiles,” *Journal of Atmospheric and Oceanic Technology*, vol. 20, no. 8, pp. 1092-1105, 2003.

[13] H. Li, Y. Ma, and Y. Yang, “Study on Retrieval of Boundary Layer Using Wavelet Transformation Method Based on Lidar Data,” *Arid Meteorology*, vol. 33, no. 1, pp. 78-88, 2015.

[14] W. P. Hooper and E. W. Eloranta, “Lidar measurements of wind in the planetary boundary layer: the method, accuracy and results from joint measurements with radiosonde and kytoon,” *Journal of climate and applied meteorology*, vol. 25, no. 7, pp. 990-1001, 1986.

[15] D. G. Steyn, M. Baldi, and R. M. Hoff, “The detection of mixed layer depth and entrainment zone thickness from lidar backscatter profiles,” *Journal of Atmospheric and Oceanic Technology*, vol. 16, no. 7, pp. 953-959, 1999.

[16] L. Wang, C. Xie, Y. Han et al., “Comparison of Retrieval Methods of Planetary Boundary Layer Height from Lidar Data,” *Journal of Atmospheric and Environmental Optics*, vol. 7, no. 4, pp. 241-247, 2012.

[17] L. Wang, C. Xie, Z. Wang et al., “Application of Gradient Method to Detect Height Distribution of Atmospheric Boundary Layer with Lidar,” *Journal of Atmospheric and Environmental Optics*, vol. 7, no. 3, pp. 161-167, 2012.

[18] C. Huang, x. Song, and Z. Liu, “Development of Atmospheric Boundary Layer Detection based on Lidar Data”, 2012.

[19] Y. Hu and Y. Gao, ”Some new knowledge to land surface processes in arid region,” *Acta Meteor Sinica*, vol. 52, no. 3, pp. 285-296, 1994.

[20] T. Tang, L. Wang, and X. Wen, “A Study of the Radiation and Surface Energy Balance Around the Ngoring Lake in Source Regions of the Yellow River,” *Journal of Glaciology and Geocryology*, vol. 35, no. 6, pp. 1462-1473, 2013.

[21]Q. Zhang and X. Cao, “The Influence of Synoptic Conditions on the Averaged Surface Heat and Radiation Budget Energy over Desert or Gobi,” *Chinese Journal of Atmospheric Sciences*, vol. 27, no. 2, pp. 245-254, 2003.

[22] J. Qiao, “The Temporal and Spatial Characteristics of Atmospheric Boundary Layer and Its Formation Mechanism over Arid Region of Northwest China,” *Chinese Academy of Meteorological Sciences*, DA, China, 2009.

[23] Q. Zhang, J. Zhang, J. Qiao et al., “Relationship of atmospheric boundary layer depth with the thermodynamic processes at the land surface in arid regions of China,” *Science China Earth Sciences*, vol. 41, no. 9, pp. 1365-1374, 2011.

[24] J. Zhang, Q. Zhang, and C. Tang, "Temporal variety of boundary layer height over deep arid region and the relations with energy balance," *Acta Ecologica Sinica*, vol. 33, no. 8, pp. 2545-2555, 2013.

[25] C. Zhao, S. Lv, Z. Li et al., "Numerical Simulation of Influence of Land Surface Thermal Condition on Badain Jaran Desert Atmospheric Boundary Layer Height in Summer," *Plateau Meteorology*, vol. 33, no. 6, pp. 1526-1533, 2014.

[26] E. J. Welton, J. R. Campbell, J. D. Spinhirne, and V. S. Scott, "Global monitoring of clouds and aerosols using a network of micropulse lidar systems," *Proc. Lidar Remote Sensing for Industry and Environmental Monitoring, Sendai, Japan, SPIE*, Vol. 4153, PP.151–158, 2001.

[27] Z. Huang, J. Huang, J. Bi et al. "Dust aerosol vertical structure measurements using three MPL lidars during 2008 China‐US joint dust field experiment," *Journal of Geophysical Research: Atmospheres (1984–2012)*, 115(D7), 2010.

[28] E. Nelson, R. Stull, and E. Eloranta, "A prognostic relation for entrainment zone thickness," *Journal of applied meteorology*, vol. 28, no. 9, pp. 885-903, 1989.

[29] H. Ding, "Measurements of aerosol vertical profiles and the mixed layer height using a micro pulse lidar," *Nanjing University of Information science & Technology*, Nanjing, DA, China, 2012.

[30] S. Zhao, L. Zhang, Z. Wang et al., "Boundary Layer Height Estimate in summer over the Lanzhou Suburb in Yuzhong Area Using Lidar Measurement and Numerical Model," *Climatic and Environmental Research*, vol. 17, no. 5, pp. 523-531, 2012.

[31] R. Wu and Y. Ma, "Comparative Analyses on Radiation Characteristic in Different Areas over the Tibetan Plateau," *Plateau Meteorology*, vol. 29, no. 2, pp. 251-259, 2010.

[32] Q. Zhang and S. Wang, "A study on atmospheric boundary layer structure on a clear Day in the arid region in Northwest China," *Acta Meteorologica Sinica*, vol. 66, no. 4, pp. 599-608, 2008.